

# First-order transition between the plaquette valence bond solid and antiferromagnetic phases of the Shastry-Sutherland model

Ning Xi,<sup>1,\*</sup> Hongyu Chen,<sup>1,\*</sup> Z. Y. Xie,<sup>1,†</sup> and Rong Yu,<sup>1,‡</sup>

<sup>1</sup>*Department of Physics and Beijing Key Laboratory of Opto-electronic Functional Materials and Micro-nano Devices, Renmin University of China, Beijing 100872, China*

We study the ground state phase diagram of the Shastry-Sutherland model by using the variational optimization of the infinite tensor network states, and find a weakly first-order transition between the plaquette and the antiferromagnetic states. The full plaquette state strongly competes with the empty plaquette ground state, with an energy difference less than  $10^{-4}J$ . We show a staggered ring exchange interaction that preserves the Shastry-Sutherland lattice symmetry can stabilize the full plaquette ground state. In light of this, we propose the triple point where the full plaquette, empty plaquette, and antiferromagnetic phases meet as a deconfined quantum critical point.

*Introduction.* Enhanced quantum fluctuations in frustrated spin system can give rise to exotic quantum phases, including quantum spin liquid (QSL), valence bond solid (VBS), and spin nematicity [1–6]. The nature of these novel quantum phases and related quantum phase transitions have been extensively studied. Though most transitions can be described within the standard Ginzburg-Landau-Wilson (GLW) paradigm, it has been proposed that the transition between a VBS and an antiferromagnetic (AFM) phase is beyond the GLW scenario, *e.g.*, via a deconfined quantum critical point (DQCP) [7]. At this point, deconfined fractionalized excitations emerge, and the enhanced symmetry allows a continuous rotation between the two distinct order parameters. However, besides some sophisticatedly designed models [8–10], it is still challenging to realize a DQCP in two-dimensional (2D) frustrated spin systems.

The Shastry-Sutherland (SS) model [11] is an ideal frustrated spin model for studying the VBS-AFM transition [12–19]. It is defined on the SS lattice as sketched in Fig 1(a), and the Hamiltonian reads

$$\hat{H}_{\text{SS}} = J \sum_{\langle i,j \rangle} \mathbf{S}_i \cdot \mathbf{S}_j + J' \sum_{\langle\langle i,j \rangle\rangle} \mathbf{S}_i \cdot \mathbf{S}_j, \quad (1)$$

where  $\mathbf{S}_i$  is an  $S = 1/2$  spin on site  $i$ ,  $J$  and  $J'$  refer to the nearest and next-nearest neighbor couplings, respectively. As demonstrated in Fig. 1(c), the ground state is found to be a product of dimer singlets (DSs) [12, 15] along the diagonal directions for  $J/J' \lesssim 0.68$ . For  $J/J' \gtrsim 0.68$ , the ground state first changes to a plaquette VBS, then to a Néel AFM with increasing  $J/J'$  [12, 15, 17]. A first-order transition between the DS and plaquette phases has been verified by various numerical results. However, the understanding of the nature of the plaquette-AFM transition remains controversial: A series expansion study [12] found a second-order transition, while an infinite projected entangled pair state (iPEPS) tensor network calculation [15] showed it to be weakly first-order. A recent DMRG study [17] proposed the transition is through a DQCP with an emergent  $O(4)$  symmetry, but another DMRG work [18] suggested a gapless

QSL settles in between the plaquette and AFM phases.

The SS model is believed to properly describe the quantum magnetism of the quasi-2D material  $\text{SrCu}_2(\text{BO}_3)_2$  [12, 20, 21]. Evidence of evolution from the DS to a plaquette then to an AFM state under pressure has been cumulated via inelastic neutron scattering (INS) [22], nuclear magnetic resonance (NMR) [23, 24], Raman scattering [25], and specific heat [26, 27] measurements. Some experimental results imply the intermediate plaquette ground state has a full plaquette (FPL) pattern, that is, the local singlet spans on the plaquette with a diagonal  $J_2$  bond [22, 25, 28]. However, numerical calculations on the SS model [15–18] suggest an empty plaquette (EPL) ground state (Fig. 1(c)). Though it was shown theoretically that the FPL can be stabilized as the ground state when the SS lattice symmetry is broken [16], the suggested symmetry breaking has not been observed. Therefore, it is still an open question how to reconcile the discrepancy between theory and experiments.

In this Letter, we investigate the ground-state phase diagram of the SS model by using a variational optimization of the infinite tensor network states with the projected entangled simplex state (PESS) construction. Our calculation clarifies the intermediate phase to be an EPL, and our results evidence a weakly first-order EPL-AFM transition at  $J/J' \approx 0.79$ , without a spin liquid phase in between. Nevertheless, the FPL state is found to be intimately competing with the EPL ground state, with an energy difference less than  $10^{-4}J$ . By including a staggered ring exchange interaction in the Hamiltonian, we show that with a perturbation that preserves the SS lattice symmetry, the ground state changes from the EPL to FPL. In light of this observation, we construct a global phase diagram of this generalized SS model, and propose the triple point among the full plaquette, empty plaquette, and antiferromagnetic phases as a deconfined quantum critical point.

*Model and method.* We consider the ground states of the SS model defined in Eq. (1). To investigate the stability of the EPL versus FPL, we also consider a generalized SS model by including a staggered ring-exchange inter-

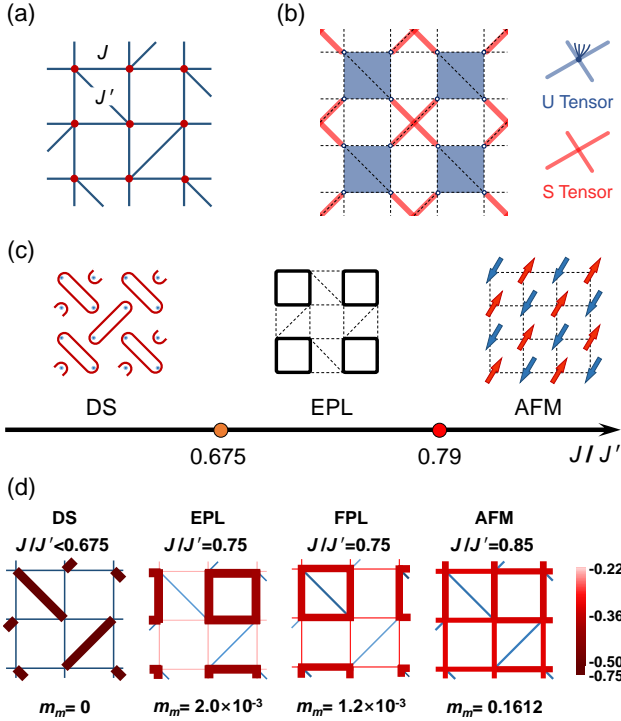


Figure 1. (a) Sketch of the SS model.  $J$  and  $J'$  refers to the nearest- and next-nearest-neighbor Heisenberg couplings. (b) The 16-PES setup on the SS lattice. The tensors are placed at the plaquette within the  $J'$  coupling. Each  $U$  tensor (blue) consists of 4 physical spin indices and 4 auxiliary ones, while an  $S$  tensor contains 4 auxiliary indices only. (c) The ground-state phase diagram of the SS model. DS, EPL, and AFM refer to dimer singlet, empty plaquette, and antiferromagnetic phases, respectively. Both the DS-EPL and EPL-AFM transitions are found to be first-order. (d) Typical configurations, corresponding spin-spin correlations and magnetic order parameters of the DS, EPL, FPL, and AFM states in the calculation. The EPL and FPL have distinct characters of symmetry breaking.

action  $\hat{H}_Q$  between the nearest neighbor spin pairs of a plaquette with  $J'$  interaction (see inset of Fig. 4(a)):

$$\hat{H}_Q = -Q \sum_{ijkl \in \square} (\mathbf{S}_i \cdot \mathbf{S}_j) (\mathbf{S}_k \cdot \mathbf{S}_l) + (\mathbf{S}_i \cdot \mathbf{S}_k) (\mathbf{S}_j \cdot \mathbf{S}_l). \quad (2)$$

The ground states are obtained by using variational optimization of the 16-PES tensor network states [29]. The PES construction of the tensor network states has been shown to give an excellent description to the ground state of frustrated spin systems [30, 31]. On the SS lattice, the 16-PES is constructed with  $U$  and  $S$  tensors as illustrated in Fig. 1(b). A projection tensor  $U$  is defined on a plaquette with the  $J'$  interaction, and carries the four spins in this plaquette. Four adjacent  $U$  tensors are then connected by an entangled simplex tensor  $S$ . The  $S$  tensor is introduced to describe the entanglement among the spin clusters but itself does not carry any physical spin degree of freedom. In this work, we find a  $2 \times 2$  unit

cell with one independent pair of  $U$  and  $S$  tensors is sufficient to characterize the ground state. The calculation is performed in an infinitely large system by employing the translational symmetry.

To determine the ground states, we adopt an advanced variational optimization method to globally minimize the ground-state energy  $\langle \psi | \hat{H} | \psi \rangle / \langle \psi | \psi \rangle$ . We are inspired by differentiable programming [32–34], which can be effectively combined with other well-developed techniques [35–39]. To be specific, the state for optimization is initialized from an arbitrary state or an approximately converged state obtained from either simple update [30, 35] or cluster update [39]. Then we use the corner transfer matrix renormalization group (CTMRG) method [36] to contract the infinite network and get the approximate environment of the local tensors. After that, we use the quasi-Newton L-BFGS algorithm to minimize the energy density, which can be effectively implemented by the Zygote package [40]. The automatic differentiation provides a global optimization strategy of the ground state, and is probably more reliable than local optimization approaches, especially for critical systems where many competing states exist.

*First-order plaquette-AFM transition.* As demonstrated in Fig. 1(c), we find the ground state is the DS for  $J/J' < 0.675$ , consistent with previous works [12, 15, 17]. Increasing  $J/J'$  the ground state first changes to the EPL, then to the AFM at  $J/J' \approx 0.79$ . To examine the plaquette-AFM transition, we calculate the ground-state energy  $E$  and its derivative  $dE/dJ$ . The results for  $D = 5$  are shown in Fig. 2(a) and (b), respectively. Though  $E$  varies smoothly across the transition,  $dE/dJ$  shows a small discontinuity at  $J/J' \approx 0.78$ , featuring a weakly first-order transition. We further calculated the order parameters  $m_m$  and  $m_p$  of the AFM and plaquette phases, respectively.

$$m_m = \sqrt{\langle m_m^x \rangle^2 + \langle m_m^y \rangle^2 + \langle m_m^z \rangle^2}, \quad (3)$$

$$m_p = \left| \sum_{\langle ij \rangle \in \square_A} \langle \mathbf{S}_i \cdot \mathbf{S}_j \rangle - \sum_{\langle ij \rangle \in \square_B} \langle \mathbf{S}_i \cdot \mathbf{S}_j \rangle \right|. \quad (4)$$

Here  $\langle m_m^\alpha \rangle = \frac{1}{N} \sum_i \langle e^{i\mathbf{Q} \cdot \mathbf{r}_i} S_{r_i}^\alpha \rangle_{r_i}$  for  $\alpha = x, y, z$  and  $\mathbf{Q} = (\pi, \pi)$ , and  $\square_{A/B}$  label the two inequivalent empty plaquettes. As shown by the solid curves with closed symbols in Fig. 2(c) and (d),  $m_m$  and  $m_p$  both exhibit small but finite abrupt jumps near  $J/J' \approx 0.78$ , consistent with the  $dE/dJ$  result. To further verify the first-order nature of the transition, we first stabilize the plaquette (AFM) state from our optimization at a  $J/J'$  ratio far from the transition, then slowly increase (decrease)  $J/J'$ . At each step, we take the converged state obtained from last step as the initial state for optimization. We repeat this procedure until the system is driven through the transition to the AFM (plaquette) phase. As shown

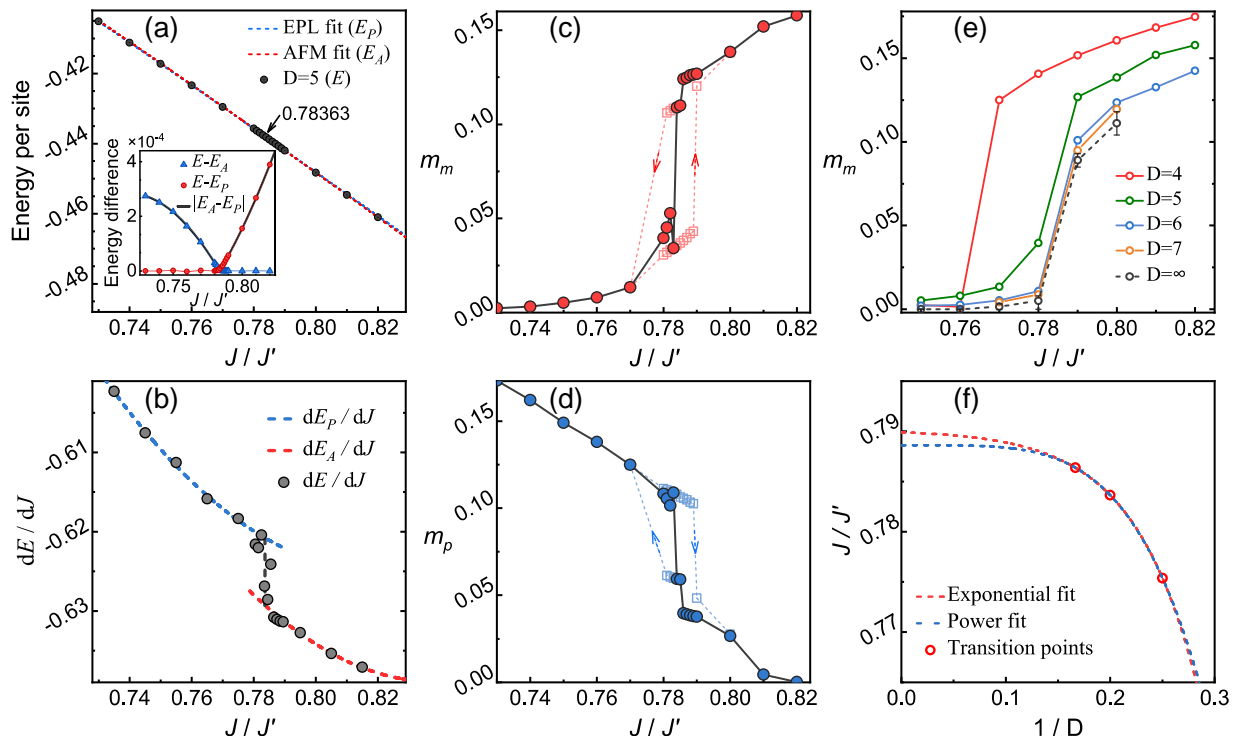


Figure 2. (a) The ground-state energy per site with  $J/J'$  at  $D = 5$ . Blue (red) dashed line is the fitted energy  $E_A$  ( $E_P$ ) in the AFM (Plaquette) phase (see text). The insert shows the energy differences  $E - E_A$  and  $E - E_P$ . (b) The first-order derivative  $dE/dJ$  with  $J/J'$  shows a clear discontinuity at the plaquette-AFM transition. (c) The staggered magnetization  $m_m$  with  $J/J'$  for  $D = 5$ . Closed circles show the  $m_m$  value of lowest energy configurations, while the open squares are obtained with biased configurations (see maintext) and exhibit clear hysteresis loop. (d) Same to (c) but for the plaquette order parameter  $m_p$ . (e) Finite- $D$  analysis and the extrapolated  $m_m$  with  $J/J'$ . (f) Extrapolation of the transition points with  $1/D$ . The transition point at each finite  $D$  is determined from the crossing point of the  $E - E_A$  and  $E - E_P$  curves in the inset of panel (a).

by the dashed curves with open symbols in Fig. 2(c) and (d), both  $m_m$  and  $m_p$  exhibit clear hysteresis loops, indicating the existence of metastable states, which is a prominent signature of a first-order transition.

This first-order transition is shown in Fig. 2(e) for all the finite  $D$  values we studied, and the large- $D$  limit is obtained by extrapolation. It shows clearly that in each curve the AFM order parameter  $m_m$  experiences a jump. Though the discontinuity  $\Delta m_m$  at the jump reduces with increasing  $D$ , it remains finite in the large- $D$  limit. This evidences a weakly first-order transition in the thermodynamic limit.

The transition point can alternatively be determined from the calculated energies at finite  $D$ . As shown in Fig. 2(a), for each  $D$  we fit the energies away from the transition ( $J/J' < 0.78$  in the plaquette phase and  $J/J' > 0.79$  in the AFM phase for  $D = 5$ ) to polynomial functions [29]. Denote  $E_P$  and  $E_A$  to be the fitted energies in the plaquette and AFM phases, respectively, and define  $\delta E_{P(A)} = E - E_{P(A)}$ . The transition point can then be accurately determined as the crossing point of  $\delta E_P$  and  $\delta E_A$ , as demonstrated in the inset of Fig. 2(a). The transition points at finite  $D$  values determined in this way are plotted in Fig. 2(f). The estimated transi-

tion points in the large- $D$  limit from two different fits are both converged to  $(J/J')_c \approx 0.79$ , which is also consistent with the value obtained from  $m_m$ .

*Nature of the plaquette ground state.* In the parameter regime  $0.68 \lesssim J/J' \lesssim 0.79$ , we are able to stabilize both two plaquette states in the calculation (see Fig. 1(d)), and we find the energy of the EPL state is always lower than that of the FPL. Interestingly, near the transition point, the energies of these two states become very close, as shown in Fig. 3(a). In the large- $D$  limit, the energy difference is less than  $10^{-4}J$ . Such a small energy difference is about the same order to the one between the EPL and AFM states near the transition (see inset of Fig. 2(a)). This implies that the FPL state, though never favored as the ground state of the SS model, emerges as a low-lying competing state near the plaquette-AFM transition. Actually, besides the FPL, we can also stabilize other metastable states with competitive energies near the transition. The emergence of these metastable states suggests enhanced low-energy fluctuations, and is consistent with the weakly first-order transition we found.

*Global phase diagram and possible DQCP.* The quasidegeneracy between the EPL and FPL states prompts that a FPL ground state can be stabilized

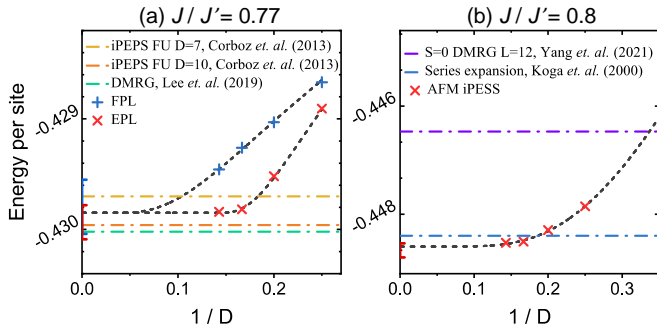


Figure 3. (a) Energies of EPL and FPL states versus  $1/D$  at  $J/J' = 0.77$ . The horizontal dashed dot lines show the plaquette ground-state energies in an iPEPS [15] and a DMRG [17] study for comparison. (b) The AFM ground-state energy versus  $1/D$  at  $J/J' = 0.8$ . The horizontal dashed dot lines show the AFM ground-state energies from another DMRG [18] and a series expansion [12] calculation for comparison.

nearby if we consider a global phase diagram with an extra tuning parameter. Such a global phase diagram would help solving the paradox on the nature of the plaquette ground state between theory and experiments. A previous theoretical work [16] found a quasi-one-dimensional singlet phase adiabatically connected to the FPL when the symmetry between the two diagonal  $J'$  bonds is broken. But the orthogonal lattice distortion accounting for this symmetry breaking has not been verified experimentally. Here we adopt a different strategy, namely, to tune the stability of the EPL and FPL phases without breaking the SS lattice symmetry. For this purpose, we generalize the SS model by including a ring-exchange-like interaction.

The model Hamiltonian reads  $\hat{H} = \hat{H}_{SS} + \hat{H}_Q$ , where  $\hat{H}_{SS}$  and  $\hat{H}_Q$  are given in Eqs. (1) and (2), respectively. The global phase diagram in the  $J$ - $Q$  plane is illustrated in Fig. 4(a). It is shown that the EPL, FPL, and AFM states span a broad regime, and the ring-exchange term  $\hat{H}_Q$  favors the FPL ground state over the EPL state. We find the FPL-AFM transition is also weakly first-order, as evidenced by the discontinuity of the ground-state energy derivative  $dE/dQ$  (Fig. 4(b) and (c)). Remarkably, going along the FPL-AFM transition trajectory toward the triple point among the EPL, FPL, and AFM phases, the discontinuity of the energy derivative reduces. It is fully suppressed when extrapolating to the triple point as shown in Fig. 4(c). This implies that the triple point is a quantum critical point. Note that our model preserves the SS lattice symmetry and the three phases break distinct symmetries. We therefore propose this point as a DQCP, because a continuous transition between any two ordered phases is prohibited within the LGW paradigm. Again, because the EPL and FPL breaks different lattice symmetries, their order parameters can be combined to a complex (two-component) monopole operator [17]. Further taking the three-component spin order parameter of

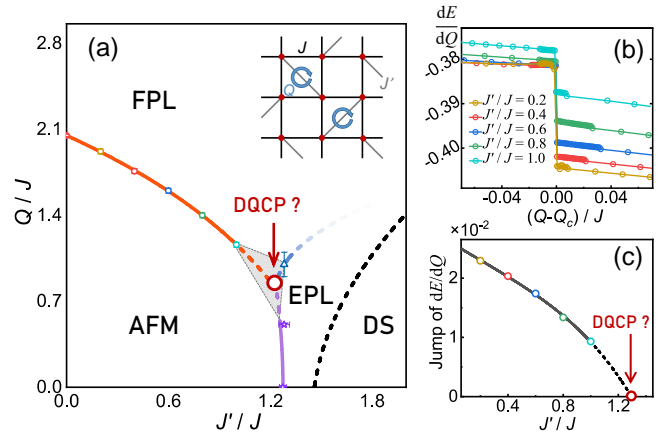


Figure 4. (a) Ground-state phase diagram of the generalized SS model that preserves the SS lattice symmetry. Besides the DS phase, EPL, FPL, and AFM phases are stabilized as the ground states. Symbols show the transition points and the lines are guides to eyes. The triple point of the EPL, FPL, and AFM phases is proposed as a DQCP (see text). Inset: Sketch of the generalized SS model with the staggered ring-exchange-like  $\hat{H}_Q$  interaction. (b) The first-order derivative of the ground-state energy  $dE/dQ$  with  $(Q - Q_c)/J$ , where  $Q_c$  is the AFM-FPL transition point. (c) The discontinuity of  $dE/dQ$  at  $Q = Q_c$  versus  $J'/J$ . The discontinuity vanishes when approaching to the triple point, implying it is a DQCP.

the AFM phase, this infers an enlarged  $SO(5)$  symmetry at the proposed DQCP.

*Discussions and conclusion.* As mentioned in the introduction, the nature of the transition between the plaquette and AFM phases is under active debate. To address this issue numerically, it is important to accurately determine the ground-state energy. In our calculations, the ground state converges quickly with increasing  $D$ . Compared to other numerical methods, as shown in Fig. 3(a), the energy of the EPL state at  $D = 6$  in our calculation is lower than that of a previous iPEPS work (Ref. [15]) for  $D = 7$ , and close to the  $D = 10$  result and a DMRG one [17]. For the AFM state shown in Fig. 3(b), the energy at  $D = 6$  in our work is lower than those of DMRG [18] and series expansion results [12].

The discontinuities of  $dE/dJ$  and  $m_m$  unambiguously show a first-order EPL-AFM transition in the SS model, and rule out a continuous transition [17] or an intermediate QSL phase [18]. The extrapolated transition points from different estimates are converged in our calculation. This suggests a QSL regime [18], even if exists, should be very narrow in the parameter space. Our results also shed light to the VBS-AFM transitions in the square lattice  $J_1$ - $J_2$  and checkerboard (CB) models [42–47], as both SS and CB models can be realized by depleting the  $J_2$  bonds from the  $J_1$ - $J_2$  model. In the CB model, the full and empty plaquettes have a larger energy difference. We then expect the VBS-AFM transition there to be stronger

first-order. In the  $J_1$ - $J_2$  model, however, the VBS-AFM transition should be weaker, or could even be intervened by an intermediate QSL, because the frustration is not released by depleting the  $J_2$  bonds.

In the shaded regime of the global phase diagram in Fig. 4, enormous competing states with close energies appear. This prevents us from locating the triple point precisely, and we cannot fully rule out a QSL in this regime. On the other hand, this suggests enhanced fluctuations which usually emerge near a QCP. Details of this phase diagram deserves future investigation.

The purpose of studying the model with the ring-exchange-like interaction in this work is to illustrate the existence of a DQCP by adding a relevant perturbation to the SS model. Certainly a realistic model for  $\text{SrCu}_2(\text{BO}_3)_2$  may contain more complicated interactions. Our argument for the DQCP is indeed generic: this intriguing physics applies to any perturbation that preserves the SS lattice symmetry and can tune the ground state between EPL and FPL. Note that a DQCP does not exist in models breaking the SS lattice symmetry [16], and our proposal obviously differs from other theoretical suggestions on realizing a DQCP in the SS model [17, 18].

In conclusion, our numerical results unambiguously show a weakly first-order plaquette-AFM transition in the SS model. Though the ground state favors the EPL configuration, the FPL is energetically competitive, and can be stabilized as the ground state under a ring-exchange-like perturbation that preserves the SS lattice symmetry. Moreover, we provide evidence for a DQCP at the triple point where the EPL, FPL, and AFM phases meet in the global phase diagram of the generalized SS model.

*Acknowledgments.* We thank fruitful discussions with Y. Cui, W. Ding, C. Liu, B. Normand, L. Wang, Y. Wang, W. Yu, and H. Zou. This work was supported by the National R&D Program of China (Grants No. 2017YFA0302900 and No. 2016YFA0300500), the National Natural Science Foundation of China (Grants No. 12174441 and No. 11774420), and the Fundamental Research Funds for the Central Universities and the Research Funds of Renmin University of China (Grants No. 18XNLG24 and No. 20XNLG19).

---

\* These authors contributed equally to this study.

† qingtaoxie@ruc.edu.cn

‡ rong.yu@ruc.edu.cn

[1] H. T. Diep *ed.*, "Frustrated Spin Systems", World Scientific (2004).  
 [2] C. Lacroix, P. Mendels, and F. Mila *ed.*, "Introduction to Frustrated Magnetism, Materials, Experiments, Theory", Springer (2010).  
 [3] L. Balents, "Spin Liquid in Frustrated Magnets", *Nature* **464**, 199 (2010).

[4] L. Savary and L. Balents, "Quantum Spin Liquids: A Review", *Rep. Prog. Phys.* **80**, 016502 (2016).  
 [5] Y. Zhou, K. Kanoda, and T.-K. Ng, "Quantum spin liquid states", *Rev. Mod. Phys.* **89**, 025003 (2017).  
 [6] R. Yu and Q. Si, "Antiferroquadrupolar and Ising-Nematic Orders of a Frustrated Bilinear-Biquadratic Heisenberg Model and Implications for the Magnetism of  $\text{FeSe}$ ", *Phys. Rev. Lett.* **115**, 116401 (2015).  
 [7] T. Senthil, A. Vishwanath, L. Balents, S. Sachdev, and M. P. A. Fisher, "Deconfined quantum critical points", *Science* **303**, 1490 (2004).  
 [8] A. W. Sandvik, "Evidence for deconfined quantum criticality in a two-dimensional heisenberg model with four-spin interactions", *Phys. Rev. Lett.* **98**, 227202 (2007).  
 [9] N. Ma *et al.*, "Dynamical signature of fractionalization at the deconfined quantum critical point", *Phys. Rev. B* **98**, 174421 (2018).  
 [10] H. Shao, W. Guo, and A. W. Sandvik, "Quantum criticality with two length scales", *Science* **352**, 213 (2016).  
 [11] B. S. Shastry and B. Sutherland, "Exact ground state of a quantum mechanical antiferromagnet", *Physica B+C* **108**, 1069 (1981).  
 [12] A. Koga and N. Kawakami, "Quantum Phase Transitions in the Shastry-Sutherland Model for  $\text{SrCu}_2(\text{BO}_3)_2$ ", *Phys. Rev. Lett.* **84**, 4461 (2000).  
 [13] C. H. Chung, J. B. Marston, and S. Sachdev, "Quantum phases of the shastry-sutherland antiferromagnet: Application to  $\text{SrCu}_2(\text{BO}_3)_2$ ", *Phys. Rev. B* **64**, 134407 (2001).  
 [14] J. H. Pixley, R. Yu, and Q. Si, "Quantum phases of the shastry-sutherland kondo lattice: Implications for the global phase diagram of heavy-fermion metals", *Phys. Rev. Lett.* **113**, 176402 (2014).  
 [15] P. Corboz and F. Mila, "Tensor network study of the shastry-sutherland model in zero magnetic field", *Phys. Rev. B* **87**, 115144 (2013).  
 [16] C. Boos, S. P. G. Crone, I. A. Niesen, P. Corboz, K. P. Schmidt, and F. Mila, "Competition between intermediate plaquette phases in  $\text{SrCu}_2(\text{BO}_3)_2$  under pressure", *Phys. Rev. B* **100**, 10 (2019).  
 [17] J. Y. Lee, Y. Z. You, S. Sachdev, and A. Vishwanath, "Signatures of a Deconfined Phase Transition on the Shastry-Sutherland Lattice: Applications to Quantum Critical  $\text{SrCu}_2(\text{BO}_3)_2$ ", *Phys. Rev. X* **9**, 11 (2019).  
 [18] J. Yang, A. W. Sandvik, and L. Wang, "Quantum criticality and spin liquid phase in the shastry-sutherland model", arXiv:2104.08887 (2021).  
 [19] K. Wierschem and P. Sengupta, "Columnar antiferromagnetic order and spin supersolid phase on the extended Shastry-Sutherland lattice", *Phys. Rev. Lett.* **110**, 207207 (2013).  
 [20] H. Kageyama, K. Yoshimura, R. Stern, N. V. Mushnikov, K. Onizuka, M. Kato, K. Kosuge, C. P. Slichter, T. Goto, and Y. Ueda, "Exact Dimer Ground State and Quantized Magnetization Plateaus in the Two-Dimensional Spin System  $\text{SrCu}_2(\text{BO}_3)_2$ ", *Phys. Rev. Lett.* **82**, 3168 (1999).  
 [21] S. Miyahara and K. Ueda, "Exact Dimer Ground State of the Two Dimensional Heisenberg Spin System  $\text{SrCu}_2(\text{BO}_3)_2$ ", *Phys. Rev. Lett.* **82**, 3701 (1999).  
 [22] M. E. Zayed *et al.*, "4-spin plaquette singlet state in the Shastry-Sutherland compound  $\text{SrCu}_2(\text{BO}_3)_2$ ", *Nat. Phys.* **13**, 962 (2017).  
 [23] T. Waki, K. Arai, M. Takigawa, Y. Saiga, Y. Uwatoko,

- H. Kageyama, and Y. Ueda, "A novel ordered phase in  $\text{SrCu}_2(\text{BO}_3)_2$  under high pressure", *J. Phys. Soc. Jpn.* **76**, 7 (2007).
- [24] S. Haravifard, D. Graf, A. E. Feiguin, C. D. Batista, J. C. Lang, D. M. Silevitch, G. Srajer, B. D. Gaulin, H. A. Dabkowska, and T. F. Rosenbaum, "Crystallization of spin superlattices with pressure and field in the layered magnet  $\text{SrCu}_2(\text{BO}_3)_2$ ", *Nat. Commun.* **7**, 1 (2016).
- [25] S. Bettler, L. Stoppel, Z. Yan, S. Gvasaliya, and A. Zheludev, "Sign switching of dimer correlations in  $\text{SrCu}_2(\text{BO}_3)_2$  under hydrostatic pressure", *Phys. Rev. Research* **2**, 012010 (2020).
- [26] J. Guo, G. Sun, B. Zhao, L. Wang, W. Hong, V. A. Sidorov, N. Ma, Q. Wu, S. Li, Z.-Y. Meng, A. W. Sandvik, and L. Sun, "Quantum Phases of  $\text{SrCu}_2(\text{BO}_3)_2$  from High-Pressure Thermodynamics", *Phys. Rev. Lett.* **124**, 206602 (2020).
- [27] J. Larrea Jiménez, S. P. G. Crone, E. Fogh, M. E. Zayed, R. Lortz, E. Pomjakushina, K. Conder, A. M. Läuchli, L. Weber, S. Wessel *et al.*, "A quantum magnetic analogue to the critical point of water", *Nature* **592**, 370 (2021).
- [28] Y. Cui *et al.*, "Proximate deconfined quantum critical point in the Shastry-Sutherland material", unpublished.
- [29] See Supplemental Material [<http://link...>] for details about the variational optimization and fitting and extrapolation, which also includes Refs. [30–32, 35, 37–41].
- [30] Z. Y. Xie, J. Chen, J. F. Yu, X. Kong, B. Normand, and T. Xiang, "Tensor renormalization of quantum many-body systems using projected entangled simplex states", *Phys. Rev. X* **4** 011025 (2014).
- [31] H. J. Liao, Z. Y. Xie, J. Chen, Z. Y. Liu, H. D. Xie, R. Z. Huang, B. Normand, and T. Xiang, "Gapless spin-liquid ground state in the  $s = 1/2$  kagome antiferromagnet", *Phys. Rev. Lett.* **118**, 137202 (2017).
- [32] H.-J. Liao, J.-G. Liu, L. Wang, and T. Xiang, "Differentiable programming tensor networks", *Phys. Rev. X* **9**, 031041 (2019).
- [33] Bin-Bin Chen, Yuan Gao, Yi-Bin Guo, Yuzhi Liu, Hui-Hai Zhao, Hai-Jun Liao, Lei Wang, Tao Xiang, Wei Li, and Z. Y. Xie, "Automatic differentiation for second renormalization of tensor networks", *Phys. Rev. B* **101**, 220409(R) (2020).
- [34] Boris Ponsioen, Fakher F. Assaad, Philippe Corboz, "Automatic differentiation applied to excitations with Projected Entangled Pair States", arXiv:2107.03399
- [35] H. C. Jiang, Z. Y. Weng, and T. Xiang, "Accurate determination of tensor network state of quantum lattice models in two dimensions", *Phys. Rev. Lett.* **101**, 090603 (2008).
- [36] P. Corboz, T. M. Rice, and M. Troyer, "Competing states in the t-J model: uniform d-wave state versus stripe state", *Phys. Rev. Lett.* **113**, 046402 (2014).
- [37] H. N. Phien, J. A. Bengua, H. D. Tuan, P. Corboz, and R. Orús, "Infinite projected entangled pair states algorithm improved: Fast full update and gauge fixing", *Phys. Rev. B* **92**, 035142 (2015).
- [38] P. Corboz, "Variational optimization with infinite projected entangled-pair states", *Phys. Rev. B* **94**, 035133 (2016).
- [39] L. Wang and F. Verstraete, "Cluster update for tensor network states", arXiv:1110.4362 (2011).
- [40] Zygote package, <https://fluxml.ai/Zygote.jl/dev/>.
- [41] F. Verstraete, and J. I. Cirac, "Renormalization algorithms for Quantum-Many Body Systems in two and higher dimensions", arXiv:cond-mat/0407066 (2004).
- [42] W.-Y. Liu, S.-S. Gong, Y.-B. Li, D. Poilblanc, W.-Q. Chen, and Z.-C. Gu, "Gapless quantum spin liquid and global phase diagram of the spin-1/2  $J_1$ - $J_2$  square antiferromagnetic Heisenberg model", arXiv:2009.01821 (2020).
- [43] L. Wang and A. W. Sandvik, "Critical level crossings and gapless spin liquid in the square-lattice spin-1/2  $J_1$ - $J_2$  Heisenberg antiferromagnet", *Phys. Rev. Lett.* **121**, 107202 (2018).
- [44] W. Brenig and A. Honecker, "Planar pyrochlore: A strong-coupling analysis", *Phys. Rev. B* **65**, 140407 (2002).
- [45] J.-B. Fouet, M. Mambrini, P. Sindzingre, and C. Lhuillier, "Planar pyrochlore: A valence-bond crystal", *Phys. Rev. B* **67**, 054411 (2003).
- [46] E. Berg, E. Altman, and A. Auerbach, "Singlet Excitations in Pyrochlore: A Study of Quantum Frustration", *Phys. Rev. Lett.* **90**, 147204 (2003).
- [47] H. Zou, F. Yang, and W. Ku, "Nearly degenerate ground states of a checkerboard antiferromagnet and their bosonic interpretation", arXiv:2011.06520 (2020).

**SUPPLEMENTAL MATERIAL – FIRST-ORDER TRANSITION BETWEEN THE PLAQUETTE VALENCE BOND SOLID AND ANTIFERROMAGNETIC PHASES OF THE SHASTRY-SUTHERLAND MODEL**

**A. Variational Optimization for the 16-PESS tensor network states**

To find the tensor-network-state representation of a target state, many optimization methods, including time evolution with simple update (SU) [30,31,35], cluster update (CU)[39], full update(FU)[37,38], and traditional variational optimization [38,41], have been developed. In this work, we adopt an advanced variational optimization of the tensor network states with the projected entangled simplex state (PESS) construction. This is inspired by the differentiable programming [32-34], which has shown great potential in the study of classical systems and quantum many-body systems. Here we construct the 16-PESS tensor network states on a square lattice as shown in Fig. 1(b) of the main text. We choose a 4-site cluster as a unit cell expressed by a  $U$  tensor. Every four adjacent units are connected by an entangled simplex tensor  $S$ . The simplex tensors  $S$  are used to describe the entanglement of these clusters. The  $U$  and  $S$  tensors are all placed at plaquettes with the  $J'$  coupling.

The optimization procedure starts from a PESS tensor network state, which can be obtained from a random initialization or a state after time evolution (combined with SU, CU, and FU). The variational process further optimizes the expectation value of the energy associated with the PESS state iteratively, until the energy is converged. The state with the lowest energy will be eventually selected as the candidate ground state of the system for a given auxiliary bond dimension  $D$ . Deep inside a phase, the nature of the ground state and the ground-state energy is not sensitive to the way of initialization. However, when the system is close to a phase transition, the converged state in usual optimization process may heavily depend on the initial states, as being trapped in local minimum is a very common problem. To relieve this issue, careful variational treatment is very important.

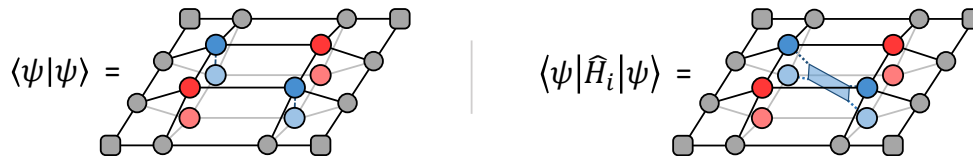


Figure S1. Tensor-diagram representation of the norm of the variational state  $\langle \psi | \psi \rangle$  and the expectation value of the local energy  $E_i = \langle \psi | \hat{H}_i | \psi \rangle / \langle \psi | \psi \rangle$ . The blue and red dots refer to the  $U$  and  $S$  tensors in the 16-PESS construction, respectively, and the grey dots denote the environment tensors constructed by CTMRG. The blue rectangle sandwiched between the two layers of network in the right panel refers to the local Hamiltonian operator  $H_i$ .

The basic idea of our variational process is to minimize the ground-state energy density  $E_i = \langle \psi | \hat{H}_i | \psi \rangle / \langle \psi | \psi \rangle$  globally. Within the 16-PESS tensor network construction,  $E_i$  and the norm of the variational state  $\langle \psi | \psi \rangle$  can be effectively evaluated, as illustrated in Fig. S1. The total ground-state energy  $E$  is then obtained by summing over the local energies. For the specific details of the optimization, we use the corner transfer matrix renormalization group (CTMRG) [38] method to contract the infinite network and get the approximate environment of the local tensors. After that, we use the quasi-Newton L-BFGS algorithm to search for the minimum of energy expectation value, in which an automatic gradient method supported by Zygote [40] is applied. This automatic differentiation program can compute  $\partial E_i / \partial U(S)$  effectively. This process involves nonlinear optimization and it is the key point for a global minimization.

When the optimization is converged, we further use the CTMRG to contract the infinite network and calculate the expectation value of energy. To obtain a more reliable extrapolation and comparison, we push the CTMRG truncation dimension  $\chi$  to a sufficiently large value. In the practical calculation, we use  $\chi$  as large as 160 for convergence. As demonstrated in Fig. S2, all the quantities are converged within  $10^{-7}$ .

**B. Fitting And Extrapolation**

We can estimate the transition point from the discontinuity of the order parameters as shown in Fig. 2 in the main text. To further confirm the result, we can use the level-crossing method described as follows, to obtain a more accurate result.

For each  $D$ , we fit the energies obtained deep in each phase to a cubic polynomial function. Define the energy difference  $\delta E_{P(A)} = E - E_{P(A)}$ , where  $E$  is the calculated energy, and  $E_{P(A)}$  is the fitted energy in the PL (AFM)

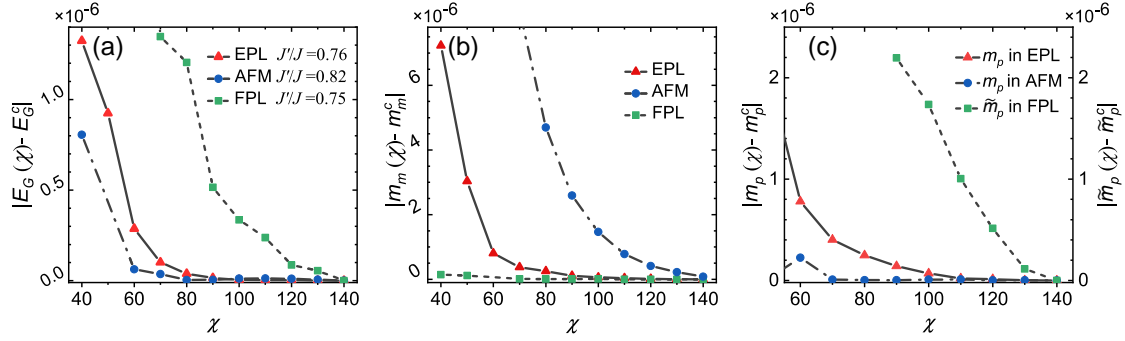


Figure S2. Convergence of expectation values versus  $\chi$  with  $D = 5$ . The corner mark  $c$  here denotes the final (convergent) value (with the largest  $\chi$  we employed). (a): Convergence of the energy as a function of  $\chi$ . (b): Convergence of the antiferromagnetic order parameter  $m_m$  as a function of  $\chi$ . (c): Convergence of the plaquette order parameters  $m_p(\tilde{m}_P)$  as a function of  $\chi$ . Here  $\tilde{m}_P$  is the order parameter of the FPL state, defined as  $\tilde{m}_P = \sum_{\langle ij \rangle \in \square} \langle \mathbf{S}_i \cdot \mathbf{S}_j \rangle - \sum_{\langle ij \rangle \in \square} \langle \mathbf{S}_i \cdot \mathbf{S}_j \rangle$  and  $m_p$  is the order parameter of the EPL state, defined in Eq. (4) of the main text.

state. The transition point can then be determined as the crossing point of  $\delta E_P$  and  $\delta E_A$  for this transition (see also main text). The crossing points for  $D=4, 5, 6$  are shown in Fig. S3, respectively. These data are then used for extrapolating the transition point in the large- $D$  limit, as shown in Fig. 2(f) of the main text. The transition point for infinite  $D$  value is then estimated to be  $J/J' \approx 0.79$  from both exponential and power-law fittings.

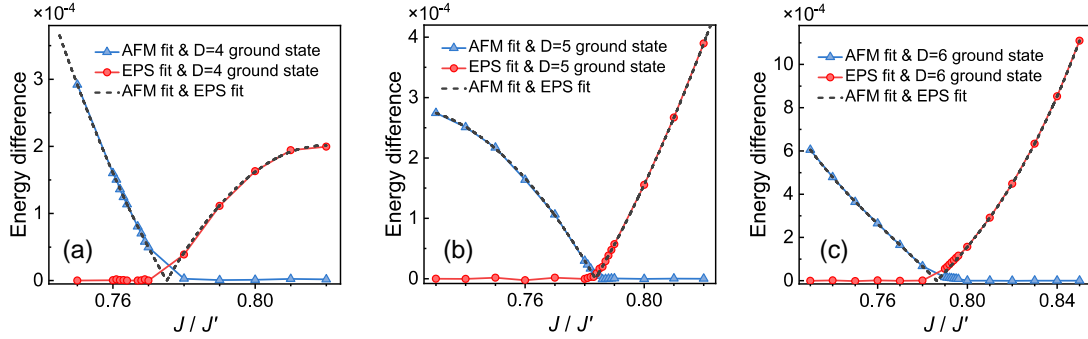


Figure S3. The energy differences  $\delta E_A$  and  $\delta E_P$  versus  $J/J'$  at  $D = 4, 5, 6$  for (a), (b), (c) respectively.